Available online at www.sciencedirect.com
SCIENCE DIRECT®
Computer Coupling of Phase Diagrams and Thermochemistry 28 (2004) 313–320
www.elsevier.com/locate/calphad

Thermodynamic description of the Cu–Mn–Zn system in the copper-rich corner

Jyrki Miettinen*

Laboratory of Metallurgy, Vuorimiehentie 2K, Helsinki University of Technology, FIN-02015 HUT, Finland

Received 19 August 2004; received in revised form 7 September 2004; accepted 8 September 2004
Available online 27 October 2004

Abstract

Thermodynamic description is presented for the ternary Cu–Mn–Zn system in its copper-rich corner. The thermodynamic parameters of the binary sub-systems, Cu–Mn and Cu–Zn, are taken from the earlier SGTE-based assessments, and those of the Mn–Zn and Cu–Mn–Zn systems are optimized in this study using the experimental phase equilibrium and thermodynamic data. The present ternary description is valid for manganese contents up to 30 wt% and zinc contents up to 60 wt%.

1. Introduction

In the present study, thermodynamic description is presented for the Cu–Mn–Zn system in its copper-rich corner. Thermodynamic data are optimized for the system using the earlier assessed data of binaries Cu–Mn [25] and Cu–Zn [20], and applying the experimental phase equilibrium data of the literature. The work includes a new optimization for the earlier assessed Mn–Zn system [21]. The study continues the recently started work for the development of a thermodynamic database for technically important copper alloys (Table 1).

2. Phases and models

Fig. 1 shows calculated phase diagrams for binaries Cu–Mn [25] and Cu–Zn [20]. They agree well with the experimental phase equilibrium data as presented in these studies. The Mn–Zn system was recently assessed by [21] but only tentatively. Hence, the system was reassessed in this study. The calculated phase diagram is presented in Fig. 2.

The phase equilibria of the Mn–Zn and Cu–Mn–Zn systems have been reviewed by [18] and [14], respectively. In the present Mn–Zn and Cu–Mn–Zn descriptions, the following phases are considered: liquid, fcc, bcc, gamma (γ), hcp, cbcc (αMn), cub (βMn), $MnZn_9$ (δ) and CuMnZn (τ). The disordered solution phases, i.e., liquid, fcc, bcc, hcp, cbcc and cub, are described with the substitutional solution model, the near-stoichiometric compounds, δ and τ, are treated as stoichiometric phases, and the ordered gamma phase is described with the substitutional solution model [22]. Worth noting is that an ordered bcc phase has been proposed to exist in systems Mn–Zn [6] and Cu–Mn–Zn [10]. However, as the quantitative experimental data for the phase is insufficient (no data are available from the Mn–Zn system and only one study [10] shows some data for the ternary system), the ordering of bcc is not considered in the present study.

By applying the substitutional solution model to the solution phases of the Cu–Mn–Zn system, the molar Gibbs energy of these phases becomes

$$\begin{aligned} G_m^\phi = {} & x_{\mathrm{Cu}}^\phi {}^oG_{\mathrm{Cu}}^\phi + x_{\mathrm{Mn}}^\phi {}^oG_{\mathrm{Mn}}^\phi + x_{\mathrm{Zn}}^\phi {}^oG_{\mathrm{Zn}}^\phi + RT(x_{\mathrm{Cu}}^\phi \ln x_{\mathrm{Cu}}^\phi \\ & + x_{\mathrm{Mn}}^\phi \ln x_{\mathrm{Mn}}^\phi + x_{\mathrm{Zn}}^\phi \ln x_{\mathrm{Zn}}^\phi) + x_{\mathrm{Cu}}^\phi x_{\mathrm{Mn}}^\phi L_{\mathrm{Cu,Mn}}^\phi \\ & + x_{\mathrm{Cu}}^\phi x_{\mathrm{Zn}}^\phi L_{\mathrm{Cu,Zn}}^\phi + x_{\mathrm{Mn}}^\phi x_{\mathrm{Zn}}^\phi L_{\mathrm{Mn,Zn}}^\phi \\ & + x_{\mathrm{Cu}}^\phi x_{\mathrm{Mn}}^\phi x_{\mathrm{Zn}}^\phi L_{\mathrm{Cu,Mn,Zn}}^\phi + {}^{\mathrm{mo}}G_m^\phi \end{aligned} \quad (1)$$

* Tel.: +35 897 735 148; fax: +35 897 735 148.
E-mail address: jyrki.miettinen@hut.fi.

0364-5916/$ - see front matter © 2004 Elsevier Ltd. All rights reserved.
doi:10.1016/j.calphad.2004.09.003

Table 1
Ternary systems Cu–X–Y of the copper alloys database

X	Y						
	Fe	Mn	Ni	Si	Sn	Zn	P
Al	[24]	[25]	F	F	[22]	[23]	
Fe		[26]	[17]	[30]			
Mn			[27]	[31]	[32]	This study	
Ni				F	[29]	[28]	
Si						F	
Sn						[23]	[29]

Earlier assessed systems are indicated by a reference code and those to be assessed within the next few years are indicated by F (future work).

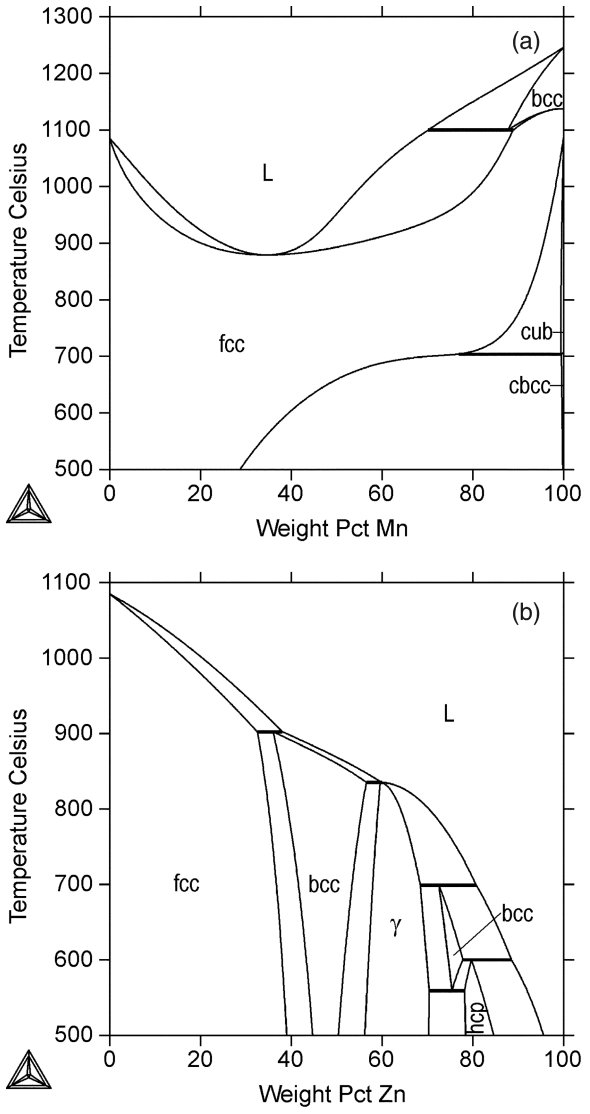

Fig. 1. Calculated phase diagrams of binaries Cu–Mn (a) and Cu–Zn (b).

where the contribution to the Gibbs energy due to the magnetic ordering, ${}^{\mathrm{mo}}G_m^{\phi}$, is expressed as

$$ {}^{\mathrm{mo}}G_m^{\phi} = RT\ln(\beta^{\phi}+1)\cdot f(\tau). \tag{2} $$

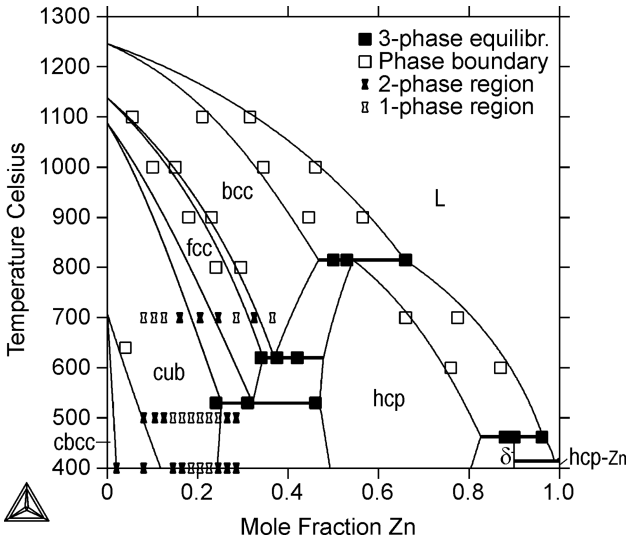

Fig. 2. Calculated Mn–Zn phase diagram, together with experimental data points [8].

In Eq. (1), R is the gas constant (8.3145 J/K mol), T is the absolute temperature, x_i is the mole fraction of component i, ${}^{o}G_i^{\phi}$ is the Gibbs energy of pure component i in phase ϕ expressed relative to the enthalpy of the component in its stable phase at 298.15 K [19], $L_{i,j}^{\phi}$ is a binary parameter describing the interaction between components i and j in phase ϕ, and $L_{\mathrm{Cu,Mn,Zn}}^{\phi}$ is a ternary interaction parameter of phase ϕ. For these parameters, ${}^{o}G_i^{\phi}$ is a function of temperature, and $L_{i,j}^{\phi}$ and $L_{\mathrm{Cu,Mn,Zn}}^{\phi}$ can be functions of temperature and composition. In Eq. (2), β^{ϕ} is a composition-dependent parameter related to the total magnetic entropy and τ is defined as $\tau = T/T_{\mathrm{C}}^{\phi}$ where T_{C}^{ϕ} is the critical temperature of magnetic ordering. For the bcc, fcc and hcp phases, the function $f(\tau)$ takes the polynomial form proposed by [13]. For other phases, ${}^{\mathrm{mo}}G_m^{\phi} = 0$.

The $MnZn_9$ phase of the binary Mn–Zn system and the CuMnZn (τ) phase of the Cu–Mn–Zn system are treated as stoichiometric phases. The Gibbs energies of formation of the phases are expressed as

$$ {}^{o}G_{\mathrm{MnZn_9}}^{\delta} = 0.1\,{}^{o}G_{\mathrm{Mn}}^{\mathrm{cbcc}} + 0.9\,{}^{o}G_{\mathrm{Zn}}^{\mathrm{hcp\_Zn}} + A + BT \tag{3} $$

$$ {}^{o}G_{\mathrm{Cu:Mn:Zn}}^{\tau} = 0.334\,{}^{o}G_{\mathrm{Cu}}^{\mathrm{fcc}} + 0.333\,{}^{o}G_{\mathrm{Mn}}^{\mathrm{cbcc}} + 0.333\,{}^{o}G_{\mathrm{Zn}}^{\mathrm{hcp\_Zn}} + A + BT \tag{4} $$

where ${}^{o}G_i^{\phi}$ is the Gibbs energy of pure component i in its stable phase at 298.15 K [19].

3. Experimental data

Okamoto and Tanner [18], and Chang et al. [14] have reviewed the earlier experimental studies on the Mn–Zn and Cu–Mn–Zn systems. Table 2 shows the experimental information selected in the present optimization. For the

Table 2
Experimental information applied in the optimization process

System	Experimental information type	Ref.
Mn–Zn	Phase equilibria	[8]
	Activity of Zn in liquid alloys, at 1573, 1523 and 1073 K	[7,12,15]
	Chemical potential of Zn in hcp alloys, at 693 K	[11]
Cu–Mn–Zn	Primary surfaces of fcc and bcc phase	[1]
	Eight isotherms, at 815, 760, 704, 672, 648, 593, 532 and 482 °C	[3–5]
	Seven isopleths, at 2.24, 5.78, 10, 15, 20, 25, 30 wt% Mn	[1,2,10]

ternary system, no experimental thermodynamic data were found from the literature.

The phase equilibrium data of the Mn–Zn system are from [8]. These data were recommended by [18] in the composition range of 0 to 60 at% Mn and at temperatures above 400 °C. At higher zinc contents, three different modifications of the ε phase (hcp) have been proposed to exist, as stated by [18], but in the present study, these are treated as one hcp phase only [8]. Also the bcc phase is treated as one phase [8], in spite of the fact that the phase may become ordered at lower temperatures [6]. This is because of the lack of accurate experimental information for the disorder-order transition of the phase.

In the case of the Cu–Mn–Zn system, there is a noticeable disagreement between the results of [10] and those of other studies [1–4]. First, the liquid phase of [10] is less stable than that of [1] (in the copper-rich corner) and the fcc phase of [10] is more stable than that in the other studies. Next, the ordering of the bcc phase has been observed by [10] only. Numerous reaction equilibria including the ordered bcc phase were reported, but at high temperatures (above 500 °C), only few measurements directly revealed the existence of the phase. Due to these differences, it was reasonable to put most weight on the data of the other studies, especially as these are quite consistent with each other. The only data adopted from [10] are the liquidus temperature data (no secondary arrest data were adopted due to the disagreement in the secondary phase) and the temperature of formation of the CuMnZn phase from the bcc phase (no data were available from other studies).

4. Thermodynamic data

The thermodynamic description of the Cu–Mn–Zn systems is presented in Table 3. The parameters marked with a reference code were adopted from the earlier SGTE assessments and those marked with *O or *E were optimized or estimated in the present study. By *O, the parameter was optimized using the experimental data of literature (Table 2) and by *E, it was estimated arbitrarily, by applying no experimental data (since not available). The

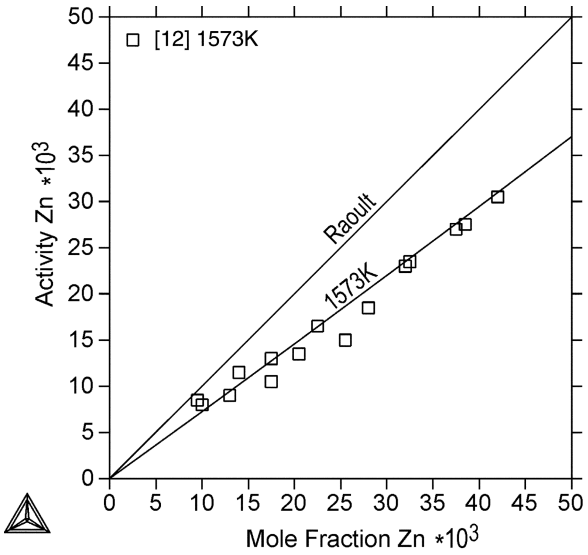

Fig. 3. Calculated activity of zinc in liquid Mn–Zn alloys at 1573 K, together with experimental data points [12]. The reference state for zinc is pure liquid Zn.

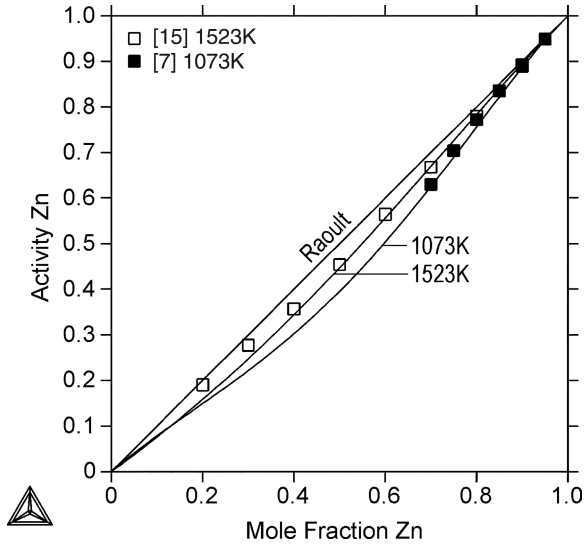

Fig. 4. Calculated activity of zinc in liquid Mn–Zn alloys at 1523 and 1073 K, together with experimental data points [7,15]. The reference state for zinc is pure liquid Zn.

thermodynamic data for the pure components are given by [19] except for the gamma phase, and the cbcc and cub phases for copper and zinc (see Table 3). The magnetic ordering parameters for the fcc, bcc and hcp phases are given as $\beta^{\mathrm{fcc}} = -1.86x_{\mathrm{Mn}}$, $\beta^{\mathrm{bcc}} = -0.27x_{\mathrm{Mn}}$, $\beta^{\mathrm{hcp}} = -1.86x_{\mathrm{Mn}}$, $T_{\mathrm{C}}^{\mathrm{fcc}} = -1620x_{\mathrm{Mn}}$, $T_{\mathrm{C}}^{\mathrm{bcc}} = -580x_{\mathrm{Mn}}$ and $T_{\mathrm{C}}^{\mathrm{hcp}} = -1620x_{\mathrm{Mn}}$ [19]. The presented ternary description is valid up to 30 wt% Mn and 60 wt% Zn.

5. Results

In the following, calculated results are compared with the original experimental data to demonstrate the successfulness

Table 3
Thermodynamic data for the Cu–Mn–Zn system obtained from the literature (reference code) and optimized (*O) or estimated (*E) in this study

	Ref.
liquid (1 sublattice, sites: 1, constituents: Cu, Mn, Zn)	
$L^{L}_{Cu,Mn} = (1800 - 2.28T) + (-6500 - 2.91T)(x_{Cu} - x_{Mn})$	[25]
$L^{L}_{Cu,Zn} = (-40\,696 + 12.653T) + (4403 - 6.554T)(x_{Cu} - x_{Zn}) + (7818 - 3.254T)(x_{Cu} - x_{Zn})^2$	[20]
$L^{L}_{Mn,Zn} = (-4800) + (10\,000 - 6T)(x_{Mn} - x_{Zn})$	*O
$L^{L}_{Cu,Mn,Zn} = (-15\,000)x_{Cu} + (-33\,000)x_{Mn} + (-33\,000)x_{Zn}$	*O
fcc (1 sublattice, sites: 1, constituents: Cu, Mn, Zn)	
$L^{fcc}_{Cu,Mn} = (11\,820 - 2.3T) + (-10\,600 + 3T)(x_{Cu} - x_{Mn}) + (0)(x_{Cu} - x_{Mn})^2 + (-4850 + 3.5T)(x_{Cu} - x_{Mn})^3$	[25]
$L^{fcc}_{Cu,Zn} = (-42\,804 + 10.023T) + (2936 - 3.053T)(x_{Cu} - x_{Zn}) + (9034 - 5.393T)(x_{Cu} - x_{Zn})^2$	[20]
$L^{fcc}_{Mn,Zn} = -9170$	*O
$L^{fcc}_{Cu,Mn,Zn} = (-5000)x_{Cu} + (-2000)x_{Mn} + (-7000)x_{Zn}$	*O
bcc (1 sublattice, sites: 1, constituents: Cu, Mn, Zn)	
$L^{bcc}_{Cu,Mn} = (11\,190 - 6T) + (-9865)(x_{Cu} - x_{Mn})$	[25]
$L^{bcc}_{Cu,Zn} = (-51\,596 + 13.064T) + (7562 - 6.454T)(x_{Cu} - x_{Zn}) + (30\,744 - 29.915T)(x_{Cu} - x_{Zn})^2$	[20]
$L^{bcc}_{Mn,Zn} = -8860$	*O
$L^{bcc}_{Cu,Mn,Zn} = (-37\,000 + 30T)x_{Cu} + (-5000)x_{Mn} + (-20\,000)x_{Zn}$	*O
gamma (γ) (1 sublattice, sites: 1, constituents: Cu, Mn, Zn)	
${}^{o}G^{\gamma}_{Cu} = 10 + {}^{o}G^{fcc}_{Cu}$	[20]
${}^{o}G^{\gamma}_{Mn} = 10 + {}^{o}G^{cbcc}_{Mn}$	[25]
${}^{o}G^{\gamma}_{Zn} = 10 + {}^{o}G^{hcp\_Zn}_{Zn}$	[20]
$L^{\gamma}_{Cu,Mn} = 50\,000$	[25]
$L^{\gamma}_{Cu,Zn} = (-39\,470 + 9.436T) + (36\,675 - 5.196T)(x_{Cu} - x_{Zn}) + (90\,163 - 32.62T)(x_{Cu} - x_{Zn})^2$	[20]
$L^{\gamma}_{Mn,Zn} = 50\,000$ (gamma not stable in binary Mn–Zn)	*E
$L^{\gamma}_{Cu,Mn,Zn^{\gamma}} = (0)x_{Cu} + (-310\,000)x_{Mn} + (-410\,000)x_{Zn}$	*O
hcp (1 sublattice, sites: 1, constituents: Cu, Mn, Zn)	
$L^{hcp}_{Cu,Mn} = 50\,000$ (hcp not stable in binary Cu–Mn)	*E
$L^{hcp}_{Cu,Zn} = (-36\,475 + 4.896T) + (24\,790 - 10.135T)(x_{Cu} - x_{Zn})$	[20]
$L^{hcp}_{Mn,Zn} = (-15\,000 + 3.9T) + (21\,000 - 9T)(x_{Mn} - x_{Zn})$	*O
$L^{hcp}_{Cu,Mn,Zn} = -75\,000$	*O
cbcc (1 sublattice, sites: 1, constituents: Cu, Mn, Zn)	
${}^{o}G^{cbcc}_{Cu} = {}^{o}G^{fcc}_{Cu} + 3556$	[25]
${}^{o}G^{cbcc}_{Zn} = {}^{o}G^{hcp\_Zn}_{Zn} + 2000$	[21]
$L^{cbcc}_{Cu,Mn} = 35\,000$	[25]
$L^{cbcc}_{Cu,Zn} = 50\,000$ (cbcc not stable in binary Cu–Zn)	*E
$L^{cbcc}_{Mn,Zn} = 5000$	*O

Table 3 (*continued*)

cub (1 sublattice, sites: 1, constituents: Cu, Mn, Zn)	
${}^{o}G^{\mathrm{cub}}_{\mathrm{Cu}} = {}^{o}G^{\mathrm{fcc}}_{\mathrm{Cu}} + 2092$	[25]
${}^{o}G^{\mathrm{cub}}_{\mathrm{Zn}} = {}^{o}G^{\mathrm{hcp\_Zn}}_{\mathrm{Zn}} + 2000$	[21]
$L^{\mathrm{cub}}_{\mathrm{Cu,Mn}} = 35\,000$	[25]
$L^{\mathrm{cub}}_{\mathrm{Cu,Zn}} = 50\,000$ (cub not stable in binary Cu–Zn)	*E
$L^{\mathrm{cub}}_{\mathrm{Mn,Zn}} = (-5200) + (-3000)(x_{\mathrm{Mn}} - x_{\mathrm{Zn}})$	*O
$MnZn_9$ (δ) (2 sublattices, sites: 0.1:0.9, constituents: Mn:Zn)	
${}^{o}G^{\delta}_{\mathrm{Mn:Zn}} = 0.1\,{}^{o}G^{\mathrm{cbcc}}_{\mathrm{Mn}} + 0.9\,{}^{o}G^{\mathrm{hcp\_Zn}}_{\mathrm{Zn}} + (-2700)$	*O
CuMnZn (τ) (3 sublattices, sites: 0.334:0.333:0.333, constituents: Cu:Mn:Zn)	
${}^{o}G^{\tau}_{\mathrm{Cu:Mn:Zn}} = 0.334\,{}^{o}G^{\mathrm{fcc}}_{\mathrm{Cu}} + 0.333\,{}^{o}G^{\mathrm{cbcc}}_{\mathrm{Mn}} + 0.333\,{}^{o}G^{\mathrm{hcp\_Zn}}_{\mathrm{Zn}} + (-10\,480)$	*O

All parameter values are in J/mol. The thermodynamic data of the pure components are taken from [19] unless a parameter expression is shown in the table.

of the optimization. The results are presented for the binary Mn–Zn system and the ternary Cu–Mn–Zn system. All calculations were carried out with the ThermoCalc software [16].

Table 4
Assessed (experimental) and calculated invariant phase equilibria of the Mn–Zn system

$\phi1$–$\phi2$–$\phi3$	T (°C)	$x^{\phi1}_{\mathrm{Zn}}$	$x^{\phi2}_{\mathrm{Zn}}$	$x^{\phi3}_{\mathrm{Zn}}$	Ref.
bcc–hcp–liq	815	0.500	0.530	0.660	Exp. [8]
	815	0.467	0.544	0.658	Cal. This study
fcc–bcc–hcp	620	0.340	0.375	0.420	Exp. [8]
	619	0.345	0.369	0.478	Cal. This study
cub–fcc–hcp	530	0.240	0.310	0.460	Exp. [8]
	531	0.253	0.322	0.470	Cal. This study
hcp–liq–$MnZn_9$	462	0.880	0.960	0.900	Exp. [8]
	463	0.827	0.964	0.900	Cal. This study
liq–$MnZn_9$–hcp_Zn	416	0.985	0.900	0.995	Exp. [8]
	414	0.989	0.900	1	Cal. This study

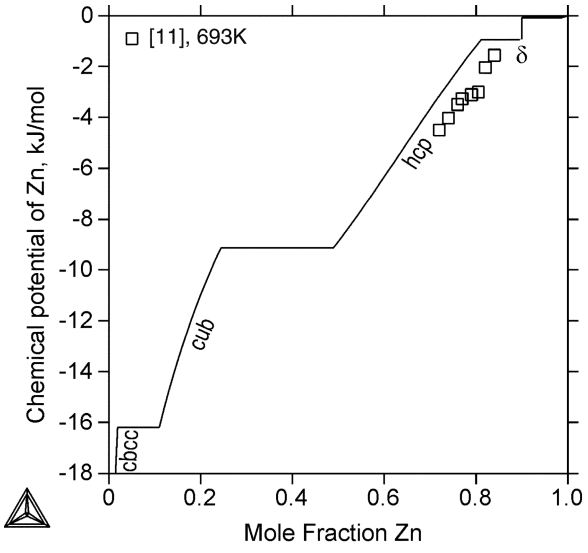

Fig. 5. Calculated chemical potential of zinc in solid Mn–Zn alloys at 693 K, together with experimental data points [11]. The reference state for zinc is pure liquid Zn.

5.1. System Mn–Zn

The Mn–Zn system was recently assessed by the author [21] but only very tentatively in the Mn-rich part of the system. In the present study, this description is extended to cover the whole system above 400 °C, by including the phase equilibria with the hcp and $MnZn_9$ (δ) phases. In the zinc-rich part of the system, there are also other phases present (three modifications of the hcp phase and some low-temperature phases) but these were excluded for the sake of simplicity. With the new data, reasonable agreement is obtained between the calculated and experimental [8] phase equilibria, as shown by the Mn–Zn phase diagram of Fig. 2 and the invariant phase equilibria of Table 4. Worth noting is that the calculated two-solid-phase regions in the Mn-rich part of the system are quite thin. Numerous trials with binary parameter optimizations were made to get them wider (agreeing better with observations) but no clear improvement was achieved. Indeed, the disagreement probably originates in the Gibbs energy data for pure Mn. Finally, Figs. 3 and 4 show calculated activities of zinc in liquid alloys and Fig. 5 shows calculated chemical potential of zinc in solid alloys. These data agree reasonably well with the experimental measurements of [7,11,12,15].

5.2. System Cu–Mn–Zn

Calculated liquidus surfaces in the copper-rich part of the system are presented in Fig. 6. The calculated lines of the liquidus isotherms agree well with the experimental data of [1]. Shown also, with the dashed line, is the

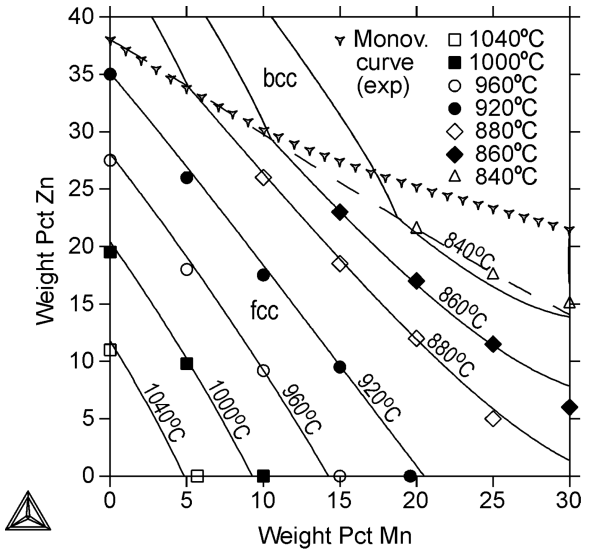

Fig. 6. Calculated liquidus surfaces in the copper-rich part of the Cu–Mn–Zn system, together with experimental data points [9] for Cu–Mn alloys and [1] for the other alloys. Shown also is the calculated (dashed line) and the experimental [1] monovariant curve of primary solidification.

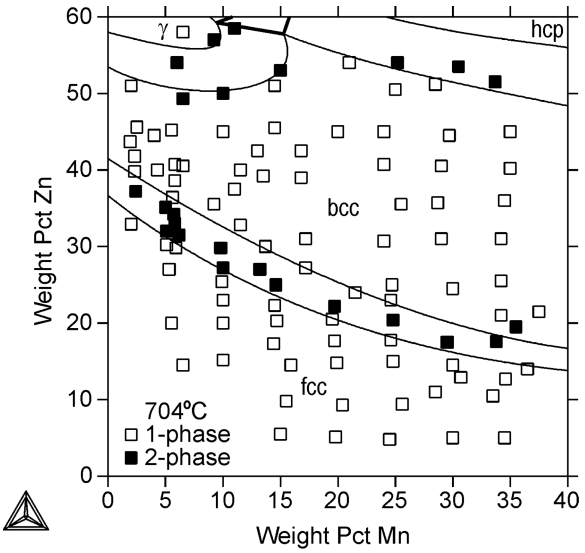

Fig. 8. Calculated isothermal section in the copper-rich part of the Cu–Mn–Zn system at 704 °C, together with experimental data points [2–4]. The measurements of [2] in region 0 to 6% Mn and 30 to 45% Zn were made at 700 °C.

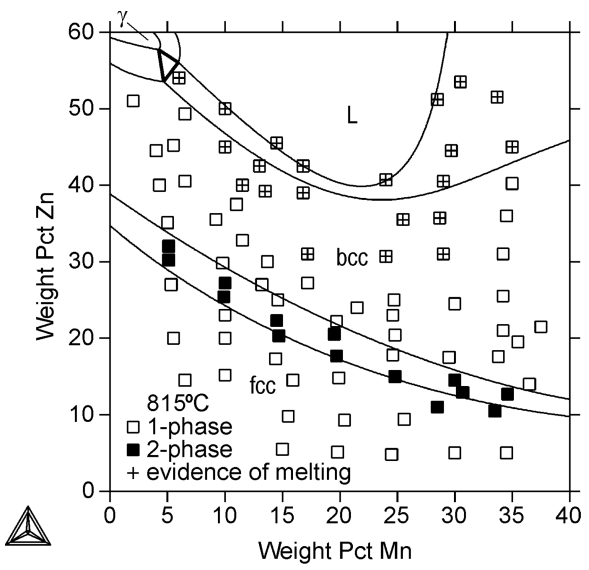

Fig. 7. Calculated isothermal section in the copper-rich part of the Cu–Mn–Zn system at 815 °C, together with experimental data points [3,4].

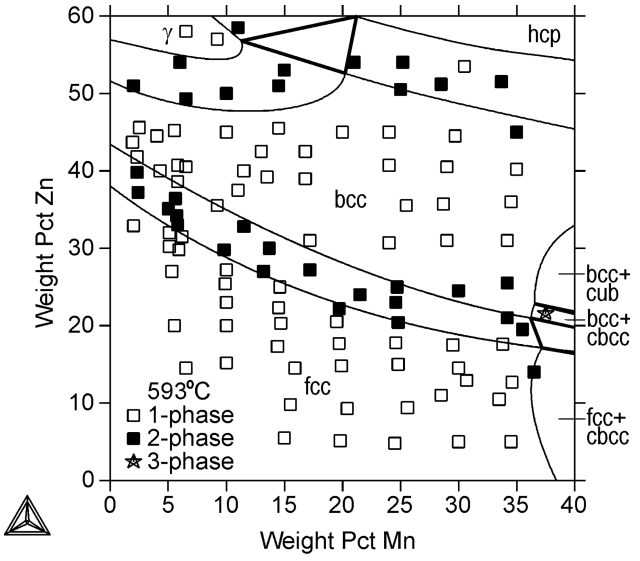

Fig. 9. Calculated isothermal section in the copper-rich part of the Cu–Mn–Zn system at 593 °C, together with experimental data points [2–4]. The measurements of [2] in region 0 to 6% Mn and 30 to 45% Zn were made at 600 °C.

calculated monovariant curve of primary solidification. This curve agrees well with the suggested curve [1] at low manganese contents but no longer at higher manganese contents. Anyway, in both cases, manganese stabilizes the bcc phase quite effectively. This tendency was not supported by [10] showing no clear effect of manganese, but the studies dealing with the solid state equilibria [3,4] unquestionably indicate that manganese must have that bcc stabilizing effect.

Figs. 7 through 10 show four calculated isothermal sections of the system, at temperatures of 815, 704, 593 and 482 °C. The agreement with the experimental data [2–4] is quite good. In Fig. 7, some experimental bcc points are equipped with a plus sign to indicate an evidence of melting for these alloys. These observations, however, are only tentative. Slight disagreement can be seen in Figs. 8 and 9, in the fcc + bcc regions at high manganese contents. A trial was made to make the calculated fcc + bcc regions "more curved" as indicated by the experimental data but this resulted in poorer agreement at lower manganese contents. Fig. 10 shows experimental points associated with fcc + X region, where X does not refer to the cbcc phase but

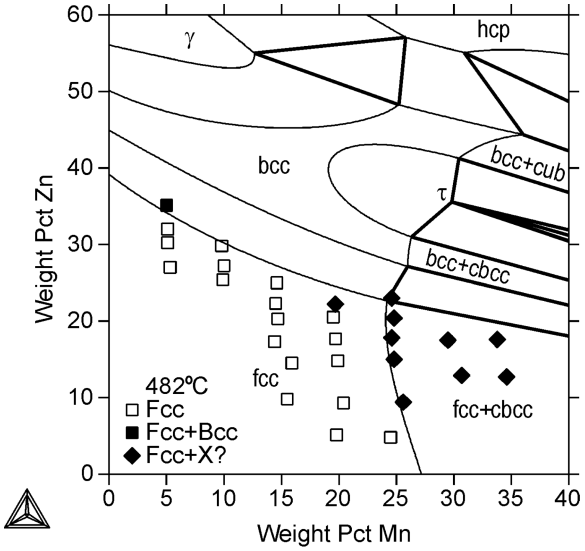

Fig. 10. Calculated isothermal section in the copper-rich part of the Cu–Mn–Zn system at 482 °C, together with experimental data points [3].

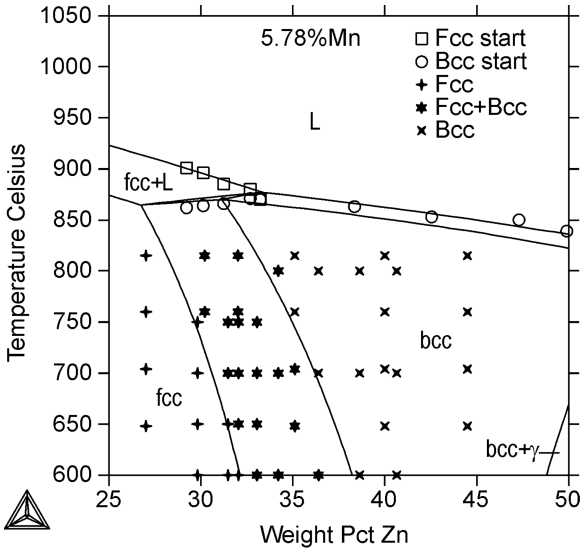

Fig. 11. Calculated isopleth at 5.78 wt% Mn in the Cu-rich part of the Cu–Mn–Zn system, together with experimental data points [2,4,10].

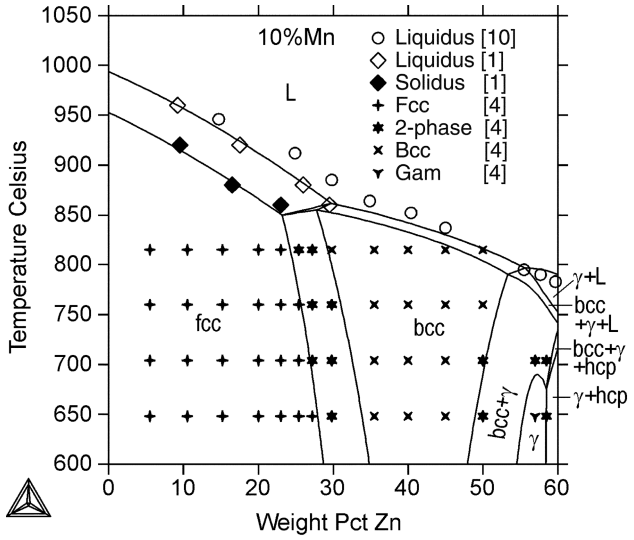

Fig. 12. Calculated isopleth at 10 wt% Mn in the Cu-rich part of the Cu–Mn–Zn system, together with experimental data points [1,4,10] (the data of [1] were read from the assessed liquidus and solidus contours).

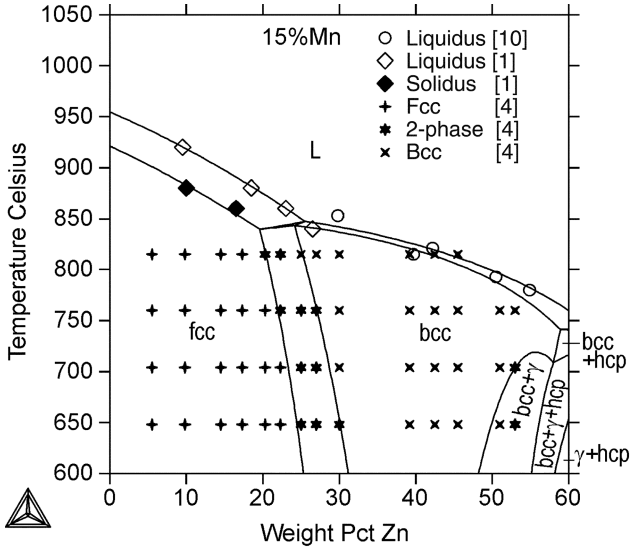

Fig. 13. Calculated isopleth at 15 wt% Mn in the Cu-rich part of the Cu–Mn–Zn system, together with experimental data points [1,4,10] (the data of [1] were read from the assessed liquidus and solidus contours).

an unidentified phase with a fcc structure [3]. However, as its constitution was not reported, the phase could not be included in the optimization. Fig. 10 also shows the presence of the CuMnZn (τ) phase. No measurements were available from [3,4] to confirm its calculated phase equilibria in Fig. 10 but [10] reported the value 502 °C for the temperature of formation of τ from the bcc phase. This single measurement was used to fix the value of the Gibbs energy of τ formation. It is worth remembering that this value is completely related to the present Gibbs energy description of the bcc phase, i.e., the value must be corrected if the bcc phase description is changed. There is still one disagreement worth mentioning, i.e., in the bcc + hcp region in Fig. 9. This disagreement originates in the narrower calculated stability region of the hcp phase in the Mn–Zn system at about 600 °C (see Fig. 2).

Finally, Figs. 11 through 15 show five calculated isopleths, at constant manganese contents of 5.78, 10, 15, 20 and 25 wt% Mn. Worth noting are the relatively high liquidus temperature values of [10] at low zinc contents but on the whole, the calculated results agree reasonably well with the experimental data of [1,2,4,10].

Calculations were also carried out for the isotherms of 760, 672, 648 and 532 °C, and for the isopleths of 2.24 and 30 wt% Mn. In each case, good agreement was obtained with the experimental data [1–5,10].

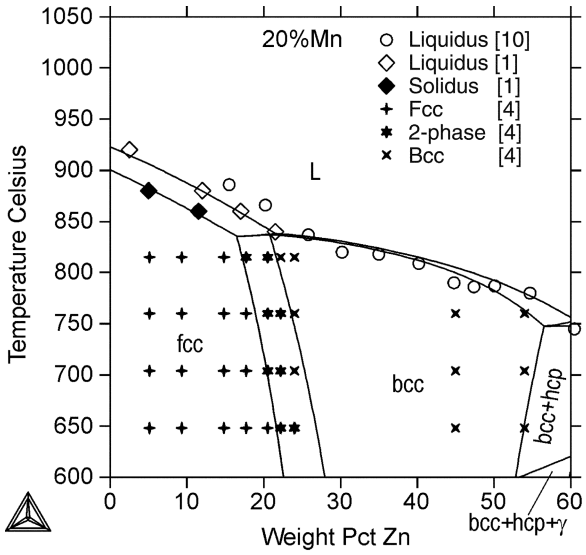

Fig. 14. Calculated isopleth at 20 wt% Mn in the Cu-rich part of the Cu–Mn–Zn system, together with experimental data points [1,4,10] (the data of [1] were read from the assessed liquidus and solidus contours).

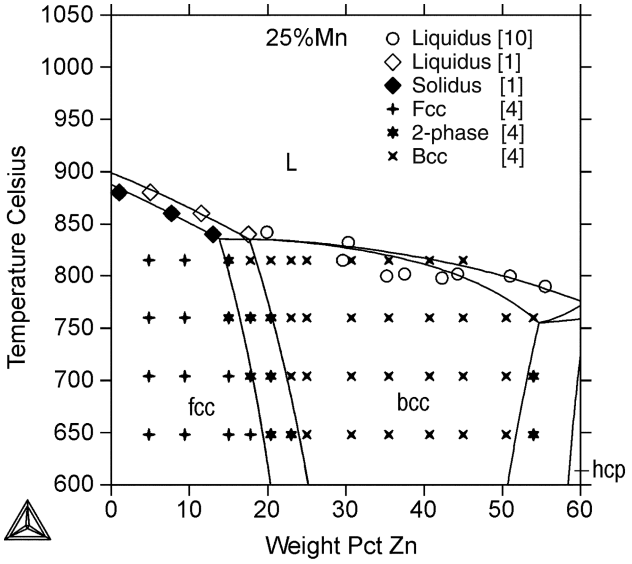

Fig. 15. Calculated isopleth at 25wt% Mn in the Cu-rich part of the Cu–Mn–Zn system, together with experimental data points [1,4,10] (the data of [1] were read from the assessed liquidus and solidus contours).

6. Summary

A thermodynamic description was optimized for the binary Mn–Zn system and the ternary Cu–Mn–Zn system applying the experimental phase equilibrium and thermodynamic data of the literature. In these descriptions, nine phases, i.e., liquid, fcc, bcc, gamma, hcp, cbcc (αMn), cub (βMn), $MnZn_9$ (δ) and CuMnZn (τ), were considered. The disordered solution phases, i.e., liquid, fcc, bcc, hcp, cbcc and cub, and the ordered gamma phase were described with the substitutional solution model, and the near-stoichiometric compounds, $MnZn_9$ and CuMnZn, were treated as stoichiometric phases. The ordered bcc phase observed in one study [10] was not considered due to the lack of accurate experimental data and the inconsistencies between that study and the other studies. In the optimization, the unary and binary thermodynamic data of the systems were taken from the recently assessed SGTE descriptions. Good or at least reasonable correlation was obtained between the calculated and the experimental thermodynamic and phase equilibrium data.

Acknowledgements

Financial support of Outokumpu Research Oy, Pori, Outokumpu Poricopper Oy, Pori, and the Technology Development Center (TEKES) during the project *Continuous casting of demanding copper alloys* (VAKU) is gratefully acknowledged.

References

[1] O. Heusler, Z. Anorg. Allg. Chem. 159 (1926) 37–54.
[2] O. Bauer, M. Hansen, Z. Metallkd. 25 (1933) 17–22.
[3] R.S. Dean, J.R. Long, T.R. Graham, A.H. Roberson, Trans. AIME 161 (1945) 232–243.
[4] T.R. Graham, J.R. Long, C.E. Armantrout, A.H. Roberson, J. Met. 1 (1949) 675–682.
[5] J.B. Haworth, W. Hume-Rothery, Phil. Mag. 43 (1952) 613–629.
[6] Y. Nakagawa, S. Sakai, T. Hori, J. Phys. Soc. Japan 17 (1962) 168–171.
[7] B.I. Lyazgin, G.N. Kazantsev, V.A. Lebedev, I.F. Nichkov, S.P. Raspopin, L.A. Martem'yanov, Zh. Fiz. Khim. 45 (1971) 1976–1978.
[8] O. Romer, E. Wachtel, Z. Metallkd. 62 (1971) 820–825.
[9] E. Schürmann, E. Schulz, Z. Metallkd. 62 (1971) 758–762.
[10] H. Watanabe, N. Kono, M. Gonda, J. Japan Inst. Met. 36 (1972) 297–305.
[11] R.P. Anantatmula, Scr. Met. 9 (1975) 223–228.
[12] I. Dimov, D. Nenov, N. Gidikova, A. Mozeva, Arch. Eisenhüettenwes. 48 (1977) 209–210.
[13] M. Hillert, M. Jarl, CALPHAD 2 (1978) 227–238.
[14] Y.A. Chang, J.P. Neumann, A. Mikula, D. Goldberg, The Metallurgy of Copper, Phase Diagrams and Thermodynamic Properties of Ternary Copper-Metal Systems, INCRA Monograph VI, 1979.
[15] E.H. Baker, Z. Metallkd. 71 (1980) 760–761.
[16] B. Sundman, B. Jansson, J.-O. Andersson, CALPHAD 9 (1985) 153–190.
[17] Å. Jansson, TRITA-MAC-0340, Materials Research Centre, Royal Institute of Technology, Stockholm, 1987.
[18] H. Okamoto, L.E. Tanner, Bull. Alloy Phase Diagr. 11 (1990) 377–384.
[19] A.T. Dinsdale, CALPHAD 15 (1991) 317–425.
[20] H. Liang, Y.A. Chang, J. Phase Equilib. 19 (1998) 25–37.
[21] J. Miettinen, CALPHAD 25 (2001) 43–58.
[22] J. Miettinen, Metall. Mater. Trans. A 33A (2002) 1639–1648.
[23] J. Miettinen, CALPHAD 26 (2002) 119–139.
[24] J. Miettinen, CALPHAD 27 (2003) 91–102.
[25] J. Miettinen, CALPHAD 27 (2003) 103–114.
[26] J. Miettinen, CALPHAD 27 (2003) 141–145.
[27] J. Miettinen, CALPHAD 27 (2003) 147–152.
[28] J. Miettinen, CALPHAD 27 (2003) 263–274.
[29] J. Miettinen, CALPHAD 27 (2003) 309–318.
[30] J. Miettinen, CALPHAD 27 (2003) 389–394.
[31] J. Miettinen, CALPHAD 27 (2003) 395–401.
[32] J. Miettinen, CALPHAD 28 (2004) 71–77.